DTU Library

Rate constant and thermochemistry for K + O2 + N2 = KO2 + N2

Sorvajärvi, Tapio; Viljanen, Jan; Toivonen, Juha; Marshall, Paul; Glarborg, Peter

[Link back to DTU Orbit](#)

Rate Constant and Thermochemistry for $K+O_2+N_2 = KO_2+N_2$

Tapio Sorvajärvi[1], Jan Viljanen[1], Juha Toivonen[1], Paul Marshall[2], Peter Glarborg[3]

[1] *Optics Laboratory, Department of Physics, Tampere University of Technology, P.O. Box 692, FI-33101 Tampere, Finland*

[2] *Department of Chemistry and Center for Advanced Scientific Computing and Modeling (CASCaM), University of North Texas, Denton, 1155 Union Circle #305070, Texas 76203–5017*

[3] *Department of Chemical and Biochemical Engineering, Technical University of Denmark, DK-2800 Kgs. Lyngby, Denmark*

The addition reaction of potassium atoms with oxygen has been studied using the collinear photofragmentation and atomic absorption spectroscopy (CPFAAS) method. KCl vapor was photolyzed with 266 nm pulses and the absorbance by K atoms at 766.5 nm was measured at various delay times with a narrow linewidth diode laser. Experiments were carried out with O_2/N_2 mixtures at a total pressure of 1 bar, over 748-1323 K. At the lower temperatures single exponential decays of [K] yielded the third-order rate constant for addition, k_{R1}, while at higher temperatures equilibration was observed in the form of double exponential decays of [K], which yielded both k_{R1} and the equilibrium constant for KO_2 formation. k_{R1} can be summarized as 1.07 x 10^{-30} $(T/1000 \text{ K})^{-0.733}$ cm^6 $molecule^{-2}$ s^{-1}. Combination with literature values leads to a recommended k_{R1} of 5.5 x 10^{-26} $T^{-1.55}$ exp(-10/T) cm^6 $molecule^{-2}$ s^{-1} over 250-1320 K, with an error limit of a factor of 1.5. A van't Hoff analysis constrained to fit the computed ΔS_{298} yields a K-O_2 bond dissociation enthalpy of 184.2 ± 4.0 kJ mol^{-1} at 298 K and $\Delta_f H_{298}(KO_2)$ = -95.2 ± 4.1 kJ mol^{-1}. The corresponding D_0 is 181.5 ± 4.0

kJ mol^{-1}. This value compares well with a CCSD(T) extrapolation to the complete basis set limit, with all electrons correlated, of 177.9 kJ mol^{-1}.

Introduction

The high-temperature chemistry of alkali species has important implications for combustion. It is well established that presence of alkali species may result in flame inhibition [1, 2] and alkali-based flame inhibitors are of interest [3, 4]. Potassium additives are also known to have an impact on gun muzzle flash [5]. Furthermore, most solid fuels contain alkali metals in minor quantities. During combustion, a portion of the alkali is released to the vapor phase, where it remains until condensing in the cooler convective regions of the boiler. Biomass such as wood and annual crops releases potassium during pyrolysis and combustion [6–8], mainly in the form of KCl. Once released, the alkali chlorides may be partially converted to alkali hydroxide or alkali sulfates [9]. During cooling the alkali components will condense, contributing to aerosol formation and/or cause operational problems, such as deposit formation and corrosion [10,11]. The fate of the alkali will depend on interactions with the sulfur and chlorine species of the gas.

Formation of potassium superoxide, KO_2, is potentially important for both flame inhibition and the high-temperature K/S/Cl transformation in combustion. The ability of alkali metals to catalyze radical removal is well documented by data from laminar premixed flames [12–25] and flow reactor experiments [26]. Alkali-based flame inhibitors are typically added as particulates [3, 4] and heterogeneous effects have been proposed; however, the inhibiting effect of alkali metals is attributed mostly to gas phase radical

removal reactions. The mechanism of inhibition is still in discussion. Under reducing conditions, results from flames [16,17,21] and from flow reactors [26] are consistent with the sequence (for K): $KOH/KCl + H \rightarrow K + H_2O/HCl$, $K + OH + M \rightarrow KOH + M$. In combustion systems, alkali chlorides and alkali hydroxides are rapidly equilibrated through the fast reaction $KCl + H_2O \rightleftharpoons KOH + HCl$ [9]. Under lean conditions, the inhibition mechanism is more uncertain. The chain-terminating recombination reaction,

$$K + O_2 + M \rightleftharpoons KO_2 + M \tag{R1}$$

has been suggested to be important [18, 27–29]. However, it has been questioned whether potassium superoxide was sufficiently stable to play an important role under flame conditions [2, 26].

Formation of alkali superoxides (mainly KO_2) may also play a role in the gas-phase transformation of alkali, sulfur and chlorine species in solid fuel combustion. Provided KO_2 is sufficiently stable, it could promote oxidation of SO_2 to SO_3 through the reaction $SO_2 + KO_2 \rightarrow SO_3 + KO$, which has been estimated to be fast [30].

The importance of KO_2 in combustion depends on the rate constant for $K + O_2 + M$ (R1) and on the thermal stability of KO_2. Values of k_{R1} have been measured directly in the temperature range 250-1100 K [31–34], inferred from studies of lean premixed flames [27–29], and calculated theoretically [35]. The direct measurements are in reasonably good agreement but deviate significantly from the values derived at high temperatures from flames. Also the thermochemistry of KO_2 is in discussion. Values for the bond dissociation energy D_0 of KO_2 have been inferred from flame studies [18,36], a molecular beam study [37], time resolved decay of atomic potassium [34], and from theory [34, 39–41]. While recent theoretical studies imply a value of the

3

BDE of approximately 172±4 kJ mol^{-1} [39–41], some data inferred from experiment indicate a substantially larger value [34, 37].

The objective of the present work is to extend the measurement range for the rate constant for K + O$_2$ + N$_2$ to higher temperatures compared to previous direct studies, and to provide the first direct measurements of the bond dissociation energy of KO$_2$. For this purpose we use the recently developed optical technique called collinear photofragmentation and atomic absorption spectroscopy (CPFAAS). This technique is based on the fragmentation of a precursor molecule and the detection of the fragment atoms via absorption spectroscopy [42, 43]. It has been applied to monitor concentrations of the precursors KCl and KOH in combustion during combustion of solid biomass fuels [44]. Previous CPFAAS studies have focused on the maximum absorbance right after the photofragmentation that is proportional to the precursor molecule concentration. The decay process of the induced K atoms has been assumed to be exponential and was not studied in detail. In the present work, measurements analogous to CPFAAS experiments are performed in order to study the decay process of [K] in the temperature range of 748-1323 K and in atmospheres containing O$_2$ from 40 ppm to 21.4%.

Experimental

Potassium atoms were produced and detected using a measurement setup presented in Fig. 1. The detected K atoms were formed through photofragmentation of KCl molecules in an 80 cm long quartz-made sample tube having an inner diameter of 35 mm. The KCl powder was brought into the middle of the cell in a 10 cm long glazed combustion boat. The temperature of the

sample tube was adjusted with a 50 cm long and 30 cm wide tube oven. The gas atmosphere in the tube was adjusted by flushing the tube for 5 minutes before each experiment with a gas mixture prepared by diluting dry synthetic air with nitrogen using a mass flow controller (5850S, Brooks Instruments). A gas flow of 2 standard liters per minute (L min^{-1}) was brought to the tube from the entrance side of the probe laser and 0.2 L min^{-1} from the exhaust side of the tube. The small flow at the exhaust side prevented the deposition of the KCl vapor on the inner surface of the exit window of the cell. The gas flows were closed 2 minutes before recording the decay process of the K atoms. The sample was in atmospheric pressure during the measurement.

The dissociation of the KCl molecules was performed by applying a fragmentation laser (FQSS 266-200, Crylas GmbH) emitting 1 ns long pulses with 20 Hz repetition rate at a wavelength of 266 nm. The laser pulses were brought to the sample tube through an 18 mm hole at the side of the oven and through the wall of the tube. The transmission of the wall material for the fragmentation wavelength was measured to be approximately 80%. The pulse energies of the fragmentation laser in the sample tube were adjusted to between 1 μJ and 80 μJ and the cross sectional 1/e diameter of the pulses over the range of 3-10 mm such that detected probe beam transmission did not drop to zero. The energy densities of the pulses in the tube were smaller than saturation intensity of KCl [45]. The pulses were slightly focused with a lens prior to the entrance hole in order to increase the concentration of the released K atoms at the lower temperatures ($<$ 873 K) when the vapor pressure of KCl was small. The pulses travelled 10 mm above the top of the combustion boat and were dumped to the back wall of the oven.

The relative concentration of the K atoms was measured by applying a narrow

line width distributed feedback diode laser (Nanoplus GmbH) emitting light at the wavelength of 766.5 nm (in air). The wavelength of the diode laser was locked to the absorption line of K atoms in a reference cell (SC-K-19 x 75-Q-W, Photonics Technologies) [43]. The probe beam having a 1/e diameter of 1 mm was aligned to travel through the tube and to cross the volume affected by the fragmentation pulses. The optical path of the probe laser beam and the fragmentation pulses were parallel to each other in the tube, which enabled a study of the decay process of the K atoms at constant temperature. The induced K atoms decreased the transmission intensity of the probe beam through the cell temporarily. The transmission waveform in the vicinity of the photofragmentation was detected applying an amplified photodiode (PDA10A, Thorlabs) and recorded using a 12-bit oscilloscope (HDO6054, LeCroy).

An example waveform measured at the temperature of 1173 K in 2.67% O_2 is presented in Fig. 2a. The photofragmentation of KCl molecules took place at t = 0, which is seen as a fast decrease in the photodiode (PD) voltage due to the increased absorption by the K atoms. The fragmentation was followed by the recovering of the transmission as the induced K atoms reacted with ambient gas molecules and the distorted gas volume approached equilibrium.

In order to study the recovery process of the K atoms the PD voltage was converted to the absorbance λL by applying Beer-Lambert law,

$$\lambda L = -\ln[I(t)/I(t < 0)] \tag{1}$$

Figure 2b shows the absorbance and its 10-fold magnification. The absorbance is directly proportional to the sample concentration and the conversion can be done when absorption length and absorption cross section are known. In the example the effective absorption length was 1 cm (UV beam

6

diameter) and the absorption cross section 1.25×10^{-16} m^2 [44], which converts the absorbance having value of 1 to a K concentration of 130 ppb. At the lower end of the temperature range studied, the absorbance was observed to follow a single exponential decay,

$$\lambda L(t > 0) = A_1 \exp(-k_1 t) \tag{2}$$

while at higher temperatures a double exponential decay process was observed,

$$\lambda L(t > 0) = A_1 \exp(-k_1 t) + A_2 \exp(-k_2 t) \tag{3}$$

Results and Discussion

At 1073 K and below simple exponential kinetics were observed, in the form of Eq. 2, which may be interpreted in terms of the scheme

$$K + O_2 \xrightarrow{k_a} KO_2 \tag{a}$$

$$K \xrightarrow{k_d} \text{loss} \tag{d}$$

k_a represents the effective second-order forward rate constant for reaction R1 and k_d accounts for loss of K atoms by processes that do not involve oxygen, such as diffusion. One would therefore expect the variation of potassium concentration with time t to follow Eq. 4,

$$[K] = [K]_0 \exp(-k_1 t) \tag{4}$$

where $k_1 = k_a[O_2] + k_d$. Figure 3 shows a plot of k_1 vs $[O_2]$, from which may be seen that the expected linear dependence on $[O_2]$ from reaction (a) is exhibited, and that the intercept is negligible, so that on the short time

7

scale of these experiments k_d is indistinguishable from zero. Details of k_1 and [O_2] measurements are provided in the Supporting Information (Table S1), and the results for the third-order rate constant k_{R1} derived as the slope k_a divided by [N_2] (corresponding to 1 bar total pressure) for 873-1073 K are listed in Table 1. Approximate, purely statistical, error limits were assessed via twice the standard deviation of the slopes of plots like Fig. 3. At 748, 773 and 823 K single measurements of k_1 were made, and divided by [O_2] and [N_2] to obtain k_{R1}. We allow 25% error limits for these points, and also for a single measurement at 1323 K where black liquor (alkali-rich waste product from pulp and paper processing) rather than KCl was the source of K atoms.

Figure 4 shows a temporal K concentration profile upon photofragmentation of the KCl molecules at a temperature of 1223 K in 10.7% O_2. In agreement with the results of Fig. 2, [K] is observed to recover to its original level in two steps. In the first phase [K] decreases fast and the 1/e relaxation time constant $1/k_1$ is found to be 270 ns (Fig. 4a). Figure 4b shows how [K] does not recover fully in the first phase and saturates to a non-zero level. Figure 4c presents how the second phase relaxation takes place in microseconds. The 1/e decay time constant for the second phase relaxation was in the example signal $1/k_2 = 40$ μs.

This double-exponential behavior, quantified in the form of Eq. 3, can be observed when reactants reversibly form an intermediate, and a reactant and/or intermediate is also lost irreversibly [46]. In the absence of oxygen the lifetime of K was observed to be of the order of 1 ms, where K atoms are lost presumably mainly by diffusion out of the probe laser beam. This lifetime is too long to be significant on the time scale of the K atom profiles when O_2 is present. Accordingly, we have interpreted the results in terms of

a simple mechanism

$$K + O_2 \xrightarrow{k_a} KO_2 \qquad\qquad (a)$$

$$KO_2 \xrightarrow{k_{-a}} K + O_2 \qquad\qquad (-a)$$

$$KO_2 \xrightarrow{k_b} \text{loss} \qquad\qquad (b)$$

k_a represents the effective second-order rate constant for K-atom addition to O_2 at a given total pressure, k_{-a} is the effective first-order dissociation rate of KO_2 and k_b is the effective first-order rate of loss of KO_2 by pathways that do not regenerate K atoms. These include diffusive loss of KO_2 although presumably this is even slower than the neglected diffusive loss of K atoms. Assuming $[O_2] >> [K]_0$, the integrated rate law may be written as [46]

$$[K] = \frac{[K]_0}{\lambda_1 - \lambda_2}((Q + \lambda_1)e^{\lambda_1 t} - (Q + \lambda_2)e^{\lambda_2 t}) \qquad\qquad (5)$$

with

$$Q = k_{-a} + k_b \qquad\qquad (6)$$

$$\lambda_1 + \lambda_2 = -Q - k_a[O_2] \qquad\qquad (7)$$

$$\lambda_1 \lambda_2 = k_b k_a[O_2] \qquad\qquad (8)$$

By comparing terms with the empirical Eq. 3 we see that the three rate constants may be derived via

$$[K]_0 = A_1 + A_2 \qquad\qquad (9)$$

$$Q = k_1 + \frac{A_1(k_2 - k_1)}{[K]_0} \qquad\qquad (10)$$

$$k_a[O_2] = k_1 + k_2 - Q \qquad\qquad (11)$$

$$k_b = \frac{k_1 k_2}{k_a[O_2]} \qquad\qquad (12)$$

$$k_{-a} = Q - k_b \qquad\qquad (13)$$

9

This analysis was applied to the double exponential data obtained over 1073-1273 K. A check on the consistency of the analysis is that the $k_a[O_2]$ term should vary linearly with $[O_2]$, while k_{-a} should be independent of $[O_2]$. Figure 5 shows the results at 1223 K and it may be seen that these conditions are met. A second check is that at 1073 K, low $[O_2]$ led to double-exponential behavior while at high $[O_2]$ the equilibrium is shifted sufficiently towards products that the back reaction is negligible, leading to single exponential decays of [K]. Data obtained both ways are tabulated for comparison, but unfortunately at this temperature neither method works very well because $k_a[O_2]$ and k_{-a} are not well-separated. The results are given in Table S1 where we report the slope of $k_a[O_2]$ vs $[O_2]$ plots constrained to pass through the origin, and the mean of the k_{-a} values. Again, k_{R1} is obtained by dividing k_a by $[N_2]$, and is listed in Table 1.

The present rate constants can be summarized as $k_{R1} = 1.07 \times 10^{-30} (T/1000 \ K)^{-0.733}$ cm^6 molecule^{-2} s^{-1} over 750-1320 K. They are in reasonable accord with the prior determinations up to 1100 K plotted on Fig. 6 but the rate coefficients do not extrapolate well to lower temperatures. An overall fit to the data of the present work together with those of Husain and Plane [32], Husain et al. [33], and Plane et al. [34] leads to a recommended k_{R1} of $5.5 \times 10^{-26} \ T^{-1.55} \exp(-10/T)$ cm^6 molecule^{-2} s^{-1} over 250-1320 K. An error limit of a factor of 1.5 includes most of the present and past measurements.

The ratio k_a/k_{-a} equals the concentration equilibrium constant K_c which is listed in Table 2, along with the thermodynamic equilibrium constant K_{eq} based on unit activity for a standard pressure of 1 bar. A van't Hoff plot for K_{eq} yields thermodynamic information for reaction R1. A potential complication is the temperature dependence of ΔH and ΔS. A correction

term to ln K_{eq} of $(\Delta H_T - \Delta H_{298})/RT - (\Delta S_T - \Delta S_{298})/R$ was added so that the slope and intercept of the van't Hoff plot in Fig. 7 correspond to $-\Delta H_{298}/R$ and $\Delta S_{298}/R$, respectively. This small correction was derived via statistical mechanics from the experimental properties of K, O_2 [47] and for KO_2 the vibrational frequencies of 1109, 307 and 304 cm^{-1} [48] and the ab initio C_{2V} geometry of Vasiliu et al. [41], a K-O distance of 2.402 x 10^{-10} m and a OKO angle of 32.52^o. The correction varied from -0.016 at 1073 K to -0.031 at 1323 K. The unconstrained linear fit corresponds to a second-law analysis and yields ΔS_{298} = -101.7 $\pm$ 9.9 J K^{-1} mol^{-1} and ΔH_{298} = -193.8 $\pm$ 11.9 kJ mol^{-1}. The error limits are 2σ and are purely the statistical uncertainty of the fit. A third-law analysis constrains the intercept to the separately estimated ΔS_{298} = 93.6 J K^{-1} mol^{-1} and yields ΔH_{298} = -184.2 $\pm$ 0.5 kJ mol^{-1}. The thermodynamic parameters agree between both methods but as expected the third-law method is more precise. Combined with ΔH_{298} = 89.0 $\pm$ 0.8 kJ mol^{-1} [47], the corresponding heat of formation of KO_2 is $\Delta_f H_{298}$ = -95.2 $\pm$ 4.1 kJ mol^{-1}. The experimental vibrational frequencies for KO_2 yield H_{298}-H_0 = 12.14 kJ mol^{-1}, and together with H_{298}-H_0 of 6.20 and 8.68 kJ mol^{-1} for K and O_2, respectively [47], we obtain the 0 K bond strength $D_0(K\text{-}O_2)$ as 181.5 kJ mol^{-1}. This value is compared with experimental and theoretical results from the literature in Table 4.

There remains the issue of systematic error. A rough-and-ready approach is based on the ca. factor of 1.5 differences between literature determinations of k_a which, if propagated as a factor of 1.5 variation in K_{eq}, imply a variation of ± 4 kJ mol^{-1} in ΔH_{298}. With this as an uncertainty limit, the 298 K bond strength is 8.7 kJ mol^{-1} above that calculated by Vasiliu et al. [41] and is therefore significantly different.

11

Ab initio analysis

It is common to exclude core electrons from the correlation treatment in ab initio analysis. For a potassium atom, these would be the 1s, 2s, 2p, 3s and 3p orbitals. However, in an ionic compound like KO_2 the potassium loses its only valence 4s electron so the remaining interactions involve the core electrons. Indeed, the 3s and 3p atomic orbitals may be higher in energy than the oxygen orbitals. For this reason it has become standard practice in calculations on alkali metals to incorporate some of these inner orbitals in the correlation space [49] and, in particular, Vasilu et al. [41] included the 3s and 3p electrons in their correlation treatment at the coupled cluster level, CCSD(T), for potassium compounds.

In this work the geometries of O_2, O_2^- and KO_2 were obtained using coupled cluster theory and the large aug-cc-pwCVQZ atomic basis set for oxygen [50] and specially constructed for potassium by Peterson and coworkers [51], with all the electrons correlated. The optimized O-O distances in the three molecules are 1.206, 1.346 and 1.345 Å, consistent with a $K^+O_2^-$ species where there is charge transfer to the oxygen. In KO_2 the computed K-O distance is 2.400 Å. Then single-point energies were derived with CCSD(T)/aug-cc-pwCV5Z theory [51], again with all electrons correlated, followed by a scalar relativistic correction Erel (mass-velocity plus Darwin terms) performed at the CISD/aug-cc-pwCVQZ level of theory. These calculations were made with the Molpro 2010 program [52] and the results are listed in Table S2. The CCSD(T) results with zeta = 4 and 5 were extrapolated to the infinite basis set limit via the relation [53]:

$$E_{inf} = (125 \cdot E_5 - 64 \cdot E_4)/61 \qquad (14)$$

Vibrational zero-point energies E_{zpe} were derived from experimental data (KO_2 [48], O_2 and O_2^- [54]). The final energies ($E_{inf} + E_{rel} + E_{zpe}$) were employed to derive 0 K enthalpy changes for the reactions in Table 3, which are coupled via the Hess cycle
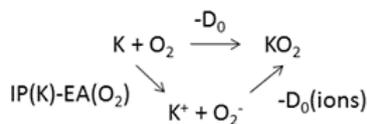
It may be seen that that the ionization potential of K is close to converged with the aug-cc-pwCVQZ basis set and that the final extrapolation is very small, only 0.09 kJ mol^{-1}, and with the relativistic correction we compute IP(K) = 418.15 kJ mol^{-1} which is 0.66 kJ mol^{-1} below the experimental value of 418.81 kJ mol^{-1} [57]. Similarly the dissociation enthalpy of KO_2 to ions is nearly converged with the zeta = 4 basis set. The other two processes involve extrapolations of only ca. 2 kJ mol^{-1} so application of different extrapolation strategies would have little impact on ΔE_{final}. The direct calculation of D_0 yields 177.9 kJ mol^{-1}, which is somewhat larger than the 172.8 kJ mol^{-1} derived by Vasilu et al. [41] using a similar computational method. The critical difference may be the use of a frozen inner core of electrons in the prior work vs. the all-electron calculations here. The 5 kJ mol^{-1} increase in D_0 more closely brings theory and experiment, 184.2±4.0 kJ mol^{-1}, into accord. The electron affinity of oxygen is reproduced well at the present level of theory, which yields EA(O_2) about 0.7 kJ mol^{-1} too low when compared to the experimental value of 43.38±0.18 kJ mol^{-1} [55, 56].

13

A similar modest error might exist in KO_2 where a superoxide moiety is present. An alternative assessment of D_0 is thus equal to D_0(ions) - IP(K) + $EA(O_2)$. With experimental values for the latter two items, this also yields $D_0 = 177.9$ kJ mol^{-1}, confirming the calculation via neutrals. The errors in IP(K) and $EA(O_2)$ have cancelled.

Conclusions

The collinear photofragmentation and atomic absorption spectroscopy (CP-FAAS) method has been applied to generate and monitor atomic potassium in the presence of oxygen. Rate constants for the third-order addition process were determined over 748-1323 K, which compare well with prior data obtained at up to 1100 K. The short time scale of the detection method permits direct observation of equilibration in the $K + O_2 = KO_2$ for the first time. A third-law analysis yields the $K-O_2$ bond dissociation enthalpy, which is 9 kJ mol^{-1} greater than the most recent ab initio calculations in the literature. We find that correlating all the electrons in coupled cluster/infinite basis set calculations roughly halves the discrepancy.

Acknowledgements

References

[1] C.R. Dautriche, *Seances Acad. Sci.* 1980, 146, 535.

[2] P. Glarborg, *Proc. Combust. Inst.* 2007, 31, 77-98.

[3] T. Mitani, T. Niioka, *Combust. Flame* 1984, 55, 13-21.

[4] H.-T. Kim, *Korean J. Chem. Eng.* 1992, 9, 1-7.

[5] G. Klingenberg, J.M. Heimerl, *Prog. Astronaut. Aeronaut.* 1992, 139, 241-260.

[6] S.C. van Lith, V.A. Ramirez, P.A. Jensen, F.J. Frandsen, P. Glarborg, *Energy Fuels* 2006, 20, 964-978.

[7] S.C. van Lith, P.A. Jensen, F.J. Frandsen, P. Glarborg, *Energy Fuels* 2008, 22, 1598-1609.

[8] J.N. Knudsen, P.A. Jensen, K. Dam-Johansen, *Energy Fuels* 2004, 18, 1385-1399.

[9] P. Glarborg and P. Marshall, *Combust. Flame* 2005, 141, 22-39.

[10] K.A. Christensen, H. Livbjerg, *J. Aerosol Sci.* 1996, 25, 185-199.

[11] K.A. Christensen, M. Stenholm, H. Livbjerg, *J. Aerosol Sci.* 1998, 29, 421-444.

[12] W.A. Rosser Jr., S.H. Inami, H. Wise, *Combust. Flame* 1963, 7, 107-119.

[13] A. van Tiggelen, M. Dewitte, J. Vrebosch, *Combust. Flame* 1964, 8, 257.

[14] W. Hoffmann, *Chemie Ing. Techn.* 1971, 43, 556-560.

[15] K.S. Iya, S. Wollowitz, W.E. Kaskan, *Proc. Combust. Inst.* 1975, 15, 329-336.

[16] D.E. Jensen, G.A. Jones, A.C.H. Mace, *J. Chem. Soc. Faraday Trans I* 1979, 75, 2377-2385.

[17] D.E. Jensen, G.A. Jones, *J. Chem. Soc. Faraday Trans. 1* 1982, 78, 2843-2850.

[18] A.J. Hynes, M. Steinberg, K. Schofield, *J. Chem. Phys.* 1984, 80, 2585-2597.

[19] H.T. Kim, J.J. Reuther, *Combust. Flame* 1984, 57, 313-317.

[20] E.M. Bulewicz, B.J. Kucnerowicz-Polak, *Combust. Flame* 1987, 70, 127-135.

[21] M. Slack, J.W. Cox, A. Grillo, R. Ryan, O. Smith, *Combust. Flame* 1989, 77, 311-320.

[22] M. Steinberg, K. Schofield, *Prog. Energy Combust. Sci.* 1990, 16, 311-317.

15

[23] K. Schofield, M. Steinberg, *J. Chem. Phys.* 1992, 96, 715-726.

[24] V. Babushok, W. Tsang, G.T. Linteris, D. Reineldt, *Combust. Flame* 1998, 115, 551.

[25] B.A. Williams, J.W. Fleming, *Proc. Combust. Inst.* 2002, 29, 345-351.

[26] L. Hindiyarti, F. Frandsen, H. Livbjerg, P. Glarborg, *Fuel* 2006, 85, 978-988.

[27] W.E. Kaskan, *Proc. Combust. Inst.* 1965, 10, 41-46.

[28] M.J. McEwan, L.F. Phillips, *Trans. Faraday Soc.* 1966, 62, 1717-1720.

[29] R. Carabetta, W.E. Kaskan, *J. Phys. Chem.* 1968, 72, 2483-2489.

[30] L. Hindiyarti, F. Frandsen, H. Livbjerg, P. Glarborg, P. Marshall, *Fuel* 2008, 87, 1591-1600.

[31] J.A. Silver, M.S. Zahniser, A.C. Stanton, C.E. Kolb, *Proc. Combust. Inst.* 1984, 20, 605-612.

[32] D. Husain, J.M.C. Plane, *J. Chem. Soc. Faraday Trans. 2* 1982, 78, 1175-1194.

[33] D. Husain, Y.H. Lee, P. Marshall, *Combust. Flame* 1987, 68, 143-154.

[34] J.M.C. Plane, B. Rajasekhar, L. Bartolotti, *J. Phys. Chem.* 1990, 94, 4161-4167.

[35] R. Patrick, D.M. Golden, *Int. J. Int. Chem.* 1984, 16, 1567-1574.

[36] D.E. Jensen, *J. Chem. Soc. Faraday Trans.* 1982, 178, 2835-2842.

[37] H. Figger, W. Schrepp, and X. Zhu, *J. Chem. Phys.* 1983, 79, 1320.

[38] M. Steinberg, K. Schofield, *J. Chem. Phys.* 1991, 94, 3901.

[39] H. Partridge, C.W. Bauschlicher Jr., M. Sodupe, S.R. Langhoff, *Chem. Phys. Lett.* 1992, 195, 200-206.

[40] E.P.F. Lee, T.G. Wright, *Chem. Phys. Lett.* 2002, 363, 139-144.

[41] M. Vasliliu, S. Li, K.A. Peterson, D. Feller, J.L. Gole, D.A.Dixon, *J. Phys. Chem. A* 2010, 114, 4272-4281.

[42] T. Sorvajärvi, J. Saarela, J. Toivonen, *Optics Lett.* 2012, 37, 4011-4013.

[43] T. Sorvajärvi, J. Toivonen, *Appl. Phys. B* 2014, 115 533-539.

[44] T. Sorvajärvi, N. DeMartini, J. Rossi, J. Toivonen, *Appl. Spectroscopy* 2014, 68, 179-187.

[45] T. Sorvajärvi, A. Manninen, J. Toivonen, J. Saarela, R. Hernberg, *Rev. Scient. Instrum.* 2009, 80, 123103

[46] Y.V. Ayhens, J.M. Nicovich, M.L. McKee, P.H. Wine, *J. Phys. Chem. A* 1997, 101, 9382-9390.

[47] The Computational Chemistry Comparison and Benchmark Database (CCCBDB), web site http://cccbdb.nist.gov/.

[48] B. Tremblay, L. Manceron, P. Roy, A.-M. LeQuéré, D. Roy, *Chem. Phys. Lett.* 1994, 228, 410-416.

[49] M.A. Iron, M. Oren, J.M.L. Martin, *Mol. Phys.* 2003, 101, 1345-1361.

[50] T.H. Dunning, Jr. *J. Chem. Phys.* 1989, 90, 1007.

[51] K.A. Peterson, private communication.

[52] H.-J. Werner, P.J. Knowles, R. Lindh, F.R. Manby, M. Schutz, P. Celani, T. Korona, A. Mitrushenkov, G. Rauhut, T.B. Adler, R.D. Amos, A. Bernhardsson, A. Berning, D.L. Cooper, M.J.O. Deegan, A.J. Dobbyn, F. Eckert, E. Goll, C. Hampel, G. Hetzer, T. Hrenar, G. Knizia, C. Köppl, Y. Liu, A.W. Lloyd, R.A. Mata, A.J. May, S.J. McNicholas, W. Meyer, M.E. Mura, A. Nicklass, P. Palmieri, K Pflüger, R. Pitzer, M. Reiher, U. Schumann, H. Stoll, A.J. Stone, R. Tarroni, T. Thorsteinsson, M. Wang, and A. Wolf. *Molpro Quantum Chemistry Package*. 2009.

[53] Halkier, A.; Helgaker, T.; Jorgensen, P.; Klopper, W.; Koch, H.; Olsen, J.; Wilson, A. K. Basis-Set Convergence in Correlated Calculations on Ne, N2, and H2O. Chem. Phys. Lett. 1998, 286, 243-252.

[54] K.M. Ervin, I. Anusiewicz, P. Skurski, J. Simons, W.C. Lineberger, *J. Phys. Chem. A* 2003, 107, 8521-8529.

[55] B. Ruscic, R.E. Pinzon, M.L. Morton, G. von Laszewski, S. Bittner, S.G. Nijsure, K.A. Amin, M. Minkoff, A.F. Wagner, *J. Phys. Chem. A* 2004, 108. 9979-9997.

[56] B. Ruscic, R.E. Pinzon, G. von Laszewski, D. Kodeboyina, A. Burcat, D. Leahy, D. Montoya, A.F. Wagner, *J. Phys. Conf. Ser.* 2005, 16, 561-570.

[57] NIST Chemistry WebBook, webbook.nist.gov/chemistry/.

T / ^{o}C	T / K	$(k_{R1} \pm 2\sigma)/10^{-30}$ cm^6 molecule^{-2} s^{-1}	Comment
475	748	1.47 ± 0.366	single point
500	773	1.31 ± 0.327	single point
550	823	1.24 ± 0.311	single point
600	873	1.18 ± 0.162	exponential decays
650	923	1.15 ± 0.0413	exponential decays
700	973	1.07 ± 0.0153	exponential decays
750	1023	0.998 ± 0.0270	exponential decays
800	1073	0.789 ± 0.140	exponential decays
800	1073	0.978 ± 0.152	equilibrium mechanism
850	1123	0.982 ± 0.0242	equilibrium mechanism
900	1173	0.969 ± 0.0319	equilibrium mechanism
950	1223	0.973 ± 0.0626	equilibrium mechanism
1000	1273	1.01 ± 0.0711	equilibrium mechanism
1050	1323	0.919 ± 0.230	single point, black liquor

Table 1: Summary of measurements for K + O$_2$ + N$_2$.

T / K	$K_c/10^{-16}$ cm^3 molecule^{-1}	K_{eq} std state 1 bar	correction^a	$\ln(K_{eq})$ + corr	σ^b
1073	23.5	1.59×10^4	-0.016	9.65	0.28
1123	7.87	5.08×10^3	-0.017	8.51	0.14
1173	3.28	2.03×10^3	-0.021	7.59	0.12
1223	1.64	971	-0.027	6.85	0.08
1273	0.799	455	-0.031	6.09	0.13

a: Equal to $(\Delta H_T - \Delta H_{298})/RT - (\Delta S_T - \Delta S_{298})/R$.

b: Statistical uncertainty in $\ln(K_{eq})$.

Table 2: Equilibrium constants derived from forward and reverse kinetics (see text).

Reaction	Δ(CCSD(T)/aug -cc-pwCVQZ)	Δ(CCSD(T)/aug -cc-pwCV5Z)	ΔE_{inf}	ΔE_{zpe}	ΔE_{rel}	ΔE_{final}
D_0(ions)	555.32	556.27	557.27	-3.92	0.91	553.35[a]
D_0	175.64	177.96	180.39	-1.11	-1.36	177.92
IP(K)	416.58	416.67	416.76	0.00	1.39	418.15
-EA(O_2)	-36.91	-38.36	-39.88	-2.81	0.88	-42.73[a]

a: Includes empirical -0.91 kJ mol^{-1} correction to the energy of O_2^- for splitting in its $^2\Pi$ ground state [54].

Table 3: Computed reaction enthalpies at 0 K in the KO_2 system, with contributions from each term, in kJ mol^{-1}.

Reference	D_0	Method
	kJ mol^{-1}	
Jensen [36]	170±30	Flame study
Figger et al. [37]	188±10	Molecular beam study
Hynes et al. [18]	174±20	Flame study
Plane et al. [34]	≥203	Time resolved decay (LIF)
Plane et al. [34]	154	Theory
Partridge et al. [39]	170±8	Theory
Lee and Wright [40]	168±3	Theory
Vasiliu et al. [41]	173	Theory
Present work	181.5±4	CPFAAS
Present work	177.9	Theory

Table 4: Reported bond dissociation energies for KO$_2$ and comparison with the present values.
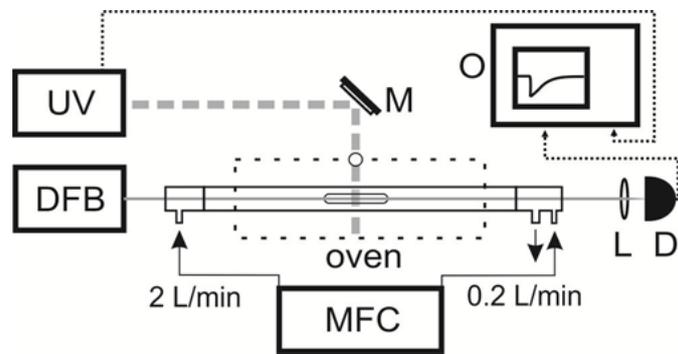
Figure 1: Experimental setup for the time resolved detection of photo-induced potassium atoms: photofragmentation laser (UV); probe laser (DFB); mirror (M); lens (L); detector (D); oscilloscope (O); mass flow controller (MFC).
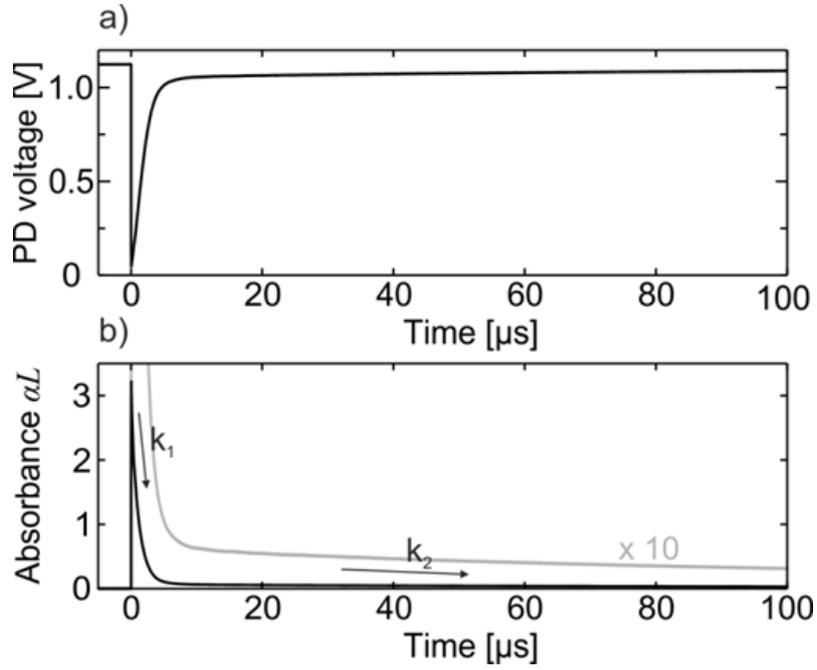
Figure 2: a) Probe laser transmission curve in the vicinity of the photofragmentation of KCl molecules and b) the decay curve of the observed absorbance due to the released K atoms. The decay takes place in two phases k_1 and k_2. The second phase decay is emphasized in b) by magnifying the decay curve with factor of 10. The experiment was done at the temperature of 1173 K in 2.67% of O_2 in N_2.
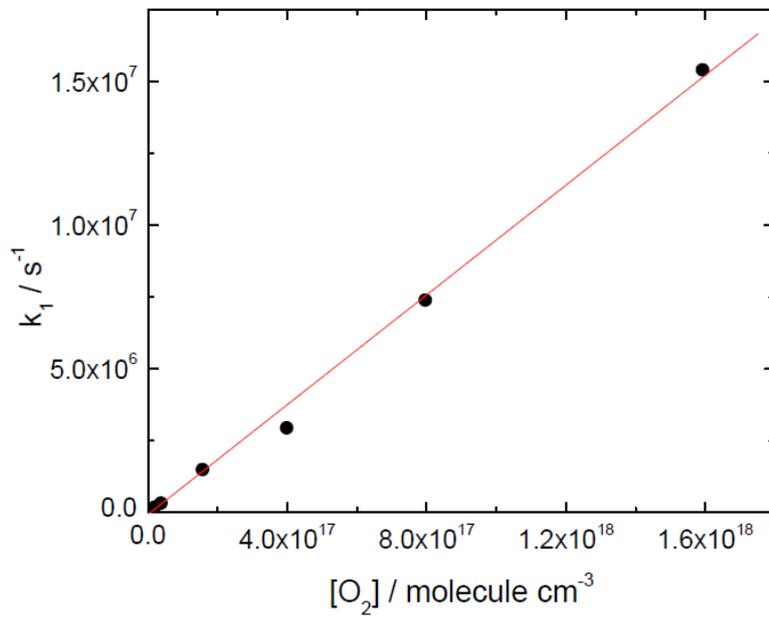
Figure 3: Exponential decay coefficient for potassium atoms as a function of oxygen concentration at 923 K and a total pressure of 1 bar made up with nitrogen.
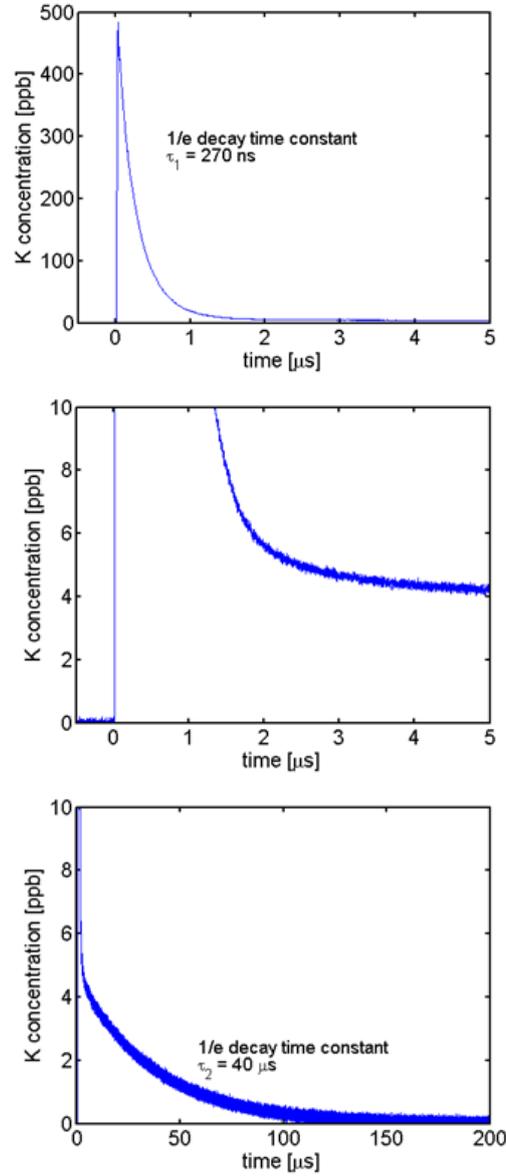
Figure 4: K relaxation after KCl photofragmentation. a) The first phase relaxation. b) The concentration of K does not reach the original background level within first 5 μs. c) The thermodynamic equilibrium [K] is reached 200 μs after the fragmentation. $[K]_0$ is the potassium concentration right after the photofragmentation, while $[K]_0^{res}$ is the concentration of the residual potassium atoms. This value is calculated by extrapolating the second phase recovery to t = 0. $\tau_1 = 1/k_1$ and $\tau_2 = 1/k_2$ are the recovery time constants in the fitting equation $[K]_t = ([K]_0 - [K]_0^{res})\exp(\text{-}t/\tau_1) + [K]_0^{res} \exp(\text{-}t/\tau_2)$.
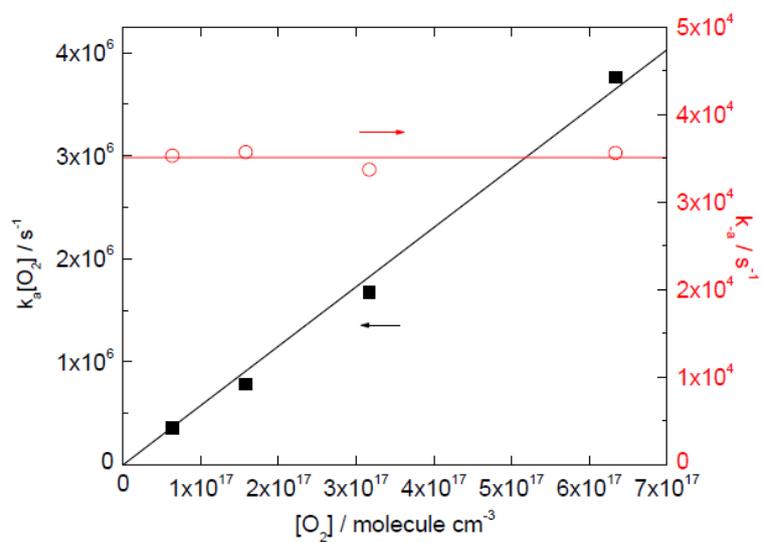
25

Figure 5: Effective first order rate constants at 1223 K for K addition to O_2 (solid black squares, left axis, linear fit constrained to pass through the origin) and for KO_2 dissociation (open red circles, right axis, linear fit constrained to have zero slope).
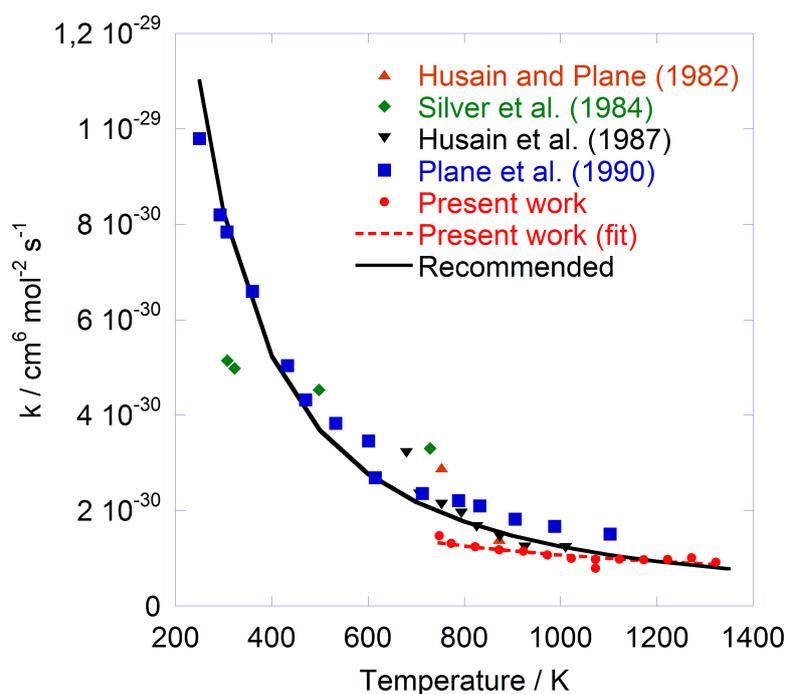
Figure 6: Arrhenius plot for the reaction $K + O_2 + N_2 \rightleftharpoons KO_2 + N_2$. The symbols denote the experimental data from Husain and Plane [32], Silver et al. [31], Husain et al. [33], Plane et al. [34] and from the present work. The dashed line shows a best fit to the present data ($k_{R1} = 1.07$ x 10^{-30} (T/1000 K)$^{-0.733}$ cm^6 molecule^{-2} s^{-1} (750-1320 K), while the solid line shows the recommended k_{R1} of 5.5 x 10^{-26} T$^{-1.55}$ exp(-10/T) cm^6 molecule^{-2} s^{-1} over 250-1320 K.
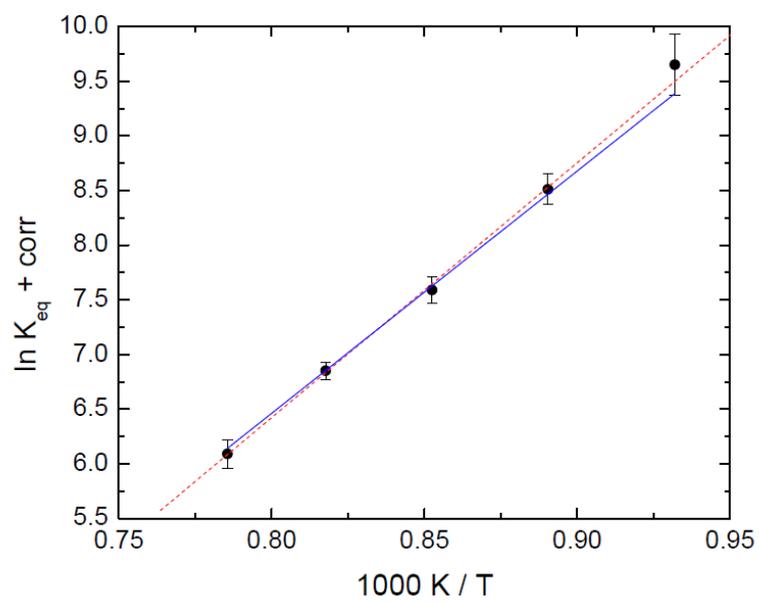
Figure 7: van't Hoff plot of K_{eq} for $K + O_2 \rightleftharpoons KO_2$. A second-law fit is shown as the dashed red line and a third-law fit is shown as the solid blue line.